

Role of non-classical paths of a photon in the density of optical states

Kritika Jain and Murugesan Venkatapathi*

Computational and Statistical Physics Laboratory, Indian Institute of Science, Bangalore, 560012

The modified density of optical states due to a weak coupling with external cavities or other resonant matter (Purcell effect), can also be recast as the effect of coherent superposition of the classical paths of the photon. When the coupling is stronger, the quantum interference of additional paths representing the possible re-absorption of the photon from the excited proximal matter, also plays a significant role in the radiative decay of the emitter. The effect of these additional non-classical paths of the photon on the density of radiative and non-radiative states, is included using a proposed simple modification to the weak coupling model. This effect is especially evident in the anomalous enhancements of spontaneous emission due to extremely small fully absorbing metal nanoparticles less than 10 nm in dimensions. Incorporating multiple emitters and such very small metal nanoparticles coupled to each other, the large contribution of non-classical paths to radiative states in such bulk materials is elucidated.

The role of vacuum modes on spontaneous emission of photons has been well elucidated and the reversible exchange of a photon between a mode of vacuum and an atom inside a micro-cavity is observable [1–4]. This Rabi oscillation of the excitation between the cavity and a resonant atom is the sign of a strongly coupled atom-vacuum system, and the coupling strength inferred by the ratio of the frequency of oscillation and the decay rate of the cavity is large ($\Omega/\Gamma > 1$). Even in the absence of the cavity i.e. weak coupling of the emitter with vacuum, when a proximal resonant object is introduced, such Rabi oscillations with the object can emerge indicating a strong coupling with matter [5–7]. The increase in decay rates due to the presence of the proximal object, is derived using the number of additional modes available for the spontaneous emission [8]. Notably, the partition of optical states into the radiative and non-radiative parts reflected the classical absorption and scattering properties of this object [9, 10]. We showed that this conventional partition results in significant anomalies when the emitter is strongly coupled to absorbing matter [11, 12]. This anomaly is also related to the large unexpected gains of emission in surface-enhanced-Raman-spectroscopy (SERS) where a strongly absorbing resonant metal structure increases the exciting radiation in the near-field by orders of magnitude, but surprisingly without apparent absorption of the emitted photons. This remarkable divergence of SERS from first principle theoretical predictions has been widening for four decades, during which the reported SERS enhancements have grown from 10^4 to 10^{14} [13–15]. Meanwhile, anomalous enhancements of spontaneous emission near fully absorbing metal nanoparticles less than 10 nm in dimensions, have also been reported [16–19].

This work has two parts. We begin with a phenomenological description of the strong coupling regime of the emitter and a nanostructure, to deduce a useful renormalization of the conventional partition of optical states into radiative and non-radiative parts [11].

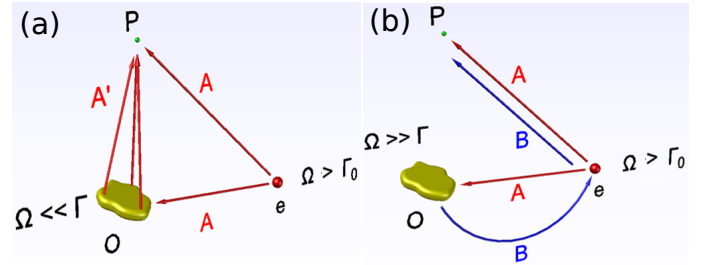


FIG. 1. Coupling of emitter e with object O and resulting coherent paths of the photon to a point P ; Ω is the frequency of emitter-object Rabi oscillations, Γ and Γ_0 are the decay rates from the object and the emitter in free-space respectively (a) Interference with classical paths represents additional decay from object (b) Interference with non-classical path B (in blue) represents coherent decay of the emitter and object.

This re-normalized partition of states is especially suited for studying bulk materials with multiple emitters and nanostructures strongly interacting with each other, as studied in this work. A first principles model of the non-Markovian interaction between a single nanoparticle and an emitter will be presented elsewhere, to validate this convenient re-normalization. In the second and more significant part of this paper, we elucidate the effect of this re-normalization on the density of radiative states in bulk-materials using detailed evaluations with many coupled emitters and metal particles.

First, we recast the modified spontaneous emission due to a body as a quantum interference of all the possible paths of the emitted photon [20–22]. This equivalent description allows us to highlight that the conventional partition of optical states into radiative and non-radiative parts is valid only for an emitter that is weakly coupled to the proximal object. We consider the effect of non-classical paths of a photon in the strong-coupling regime, which include the re-absorption of a photon by the emitter that would have otherwise dissipated in the object. Interestingly, this permits a fully *absorbing* object to increase the efficiency of spontaneous

* muruges@iisc.ac.in

emission. The quantum interference of these additional non-classical paths and the resulting effects on the radiative and non-radiative decay channels can be explained succinctly using figure 1.

When the frequency of Rabi oscillations with the object is significantly less than the decay rate of the emitter in free-space i.e. $\Omega \ll \Gamma_o$, the interaction is incoherent and the emitter is uncoupled, and we observe no effect of the object on the emission. When the resonant object is relatively close to the emitter, the increase in coupling strength [23] and a reversal of the above inequality to $\Gamma \gg \Omega > \Gamma_o$, renders the classical paths AA' through the object and the direct free-space path A shown in figure 1a, indistinguishable. It is well known that the interference of these paths over all points P given by the superposition of the scattered field from the object and incident field from the emitter, provides us the additional radiative and non-radiative optical states due to the object [24]. But note that this path A' is relevant only when the decay from the object is significantly faster than the Rabi oscillations ($\Gamma \gg \Omega$). The above condition signifies the weak coupling of the emitter with the object.

However, when the emitter is strongly coupled to the object ($\Gamma \ll \Omega$), paths A' become irrelevant as Rabi oscillations are much faster than the decay in the object. The dominant path of the photon through the object is now path B, and its interference with A as shown in figure 1b should be of primary interest. The crucial difference in this path is that there is no decay in the metal and hence no absorption. In case the probabilities of both these paths are comparable ($\Gamma \sim \Omega$), the two cases of interference (1a and 1b) can be averaged with the corresponding probabilities of these mutually exclusive paths given by $1 - e^{-\frac{\Gamma}{\Omega}}$ and $e^{-\frac{\Gamma}{\Omega}}$ [11].

Let Γ_o^r and Γ_o^{nr} be the known radiative and non-radiative decay rates of the isolated emitter adding to Γ_o . Γ^r and Γ^{nr} be the corresponding decay rates of the object adding to the total metallic contribution Γ . The total radiative and non-radiative rates of the system are a sum of the free-space and metallic components. Due to the strong coupling and the large probability of path B, the decay rates Γ^r and Γ^{nr} of the object evaluated using only paths A' have to be renormalized. The coherent decay of the emitter and object through path B, where dissipation is absent, carries more significance for the dipole mode of the object that represents its coupling to vacuum modes [11]. The substitution of the paths A' with path B, replaces non-radiative decay of the object's dipole mode numbered '1' with radiative decay. Using the probability of this path B given by $e^{-\frac{\Gamma}{\Omega}}$, the renormalized partition of decay rates is given by:

$$\Gamma_{leak} = e^{-\frac{\Gamma}{\Omega}} \cdot \Gamma_1^{nr} \quad (1)$$

The effective decay rates are:

$$\begin{aligned} \Gamma_{eff}^r &= \Gamma_o^r + \Gamma^r + \Gamma_{leak} \\ \Gamma_{eff}^{nr} &= \Gamma_o^{nr} + \Gamma^{nr} - \Gamma_{leak} \end{aligned} \quad (2)$$

Now we briefly revisit the conventional evaluation of the above decay rates and Rabi frequencies for a single emitter, before we proceed to multiple interacting emitters and metal nanoparticles. The cumulative effect of interference of the paths of a photon over all spatial points P i.e. superposition of scattered field of object and incident field of emitter, and the increase in the density of optical states, can be evaluated using the self-interaction of the emitter due to the presence of the object. The additional self-energy of the emitter at \mathbf{r}_o due to a nanostructure is:

$$\Sigma(\omega) = \frac{-2\pi q^2 \omega}{mc^2} \mathbf{e}_o \cdot \mathbf{G}(\mathbf{r}_o, \mathbf{r}_o; \omega) \cdot \mathbf{e}_o \quad (3)$$

and the above can be integrated over polarization vectors \mathbf{e}_o , and over frequency ω if required. Green dyad \mathbf{G} represents the additional self-interaction due to the nanostructure. Here q is the oscillating charge, m is its mass, and c is speed of light. The increase in decay rate due to the structure is given by imaginary part i.e. $\Gamma = -2\Im(\Sigma)$ where the reduced Planck's constant was divided out of the self-energy in equation(3). This model represents a dipole approximation of a two-level emitter in the weak vacuum-coupling regime, and it uses the Fermi golden rule to relate the decay rates to the density of optical states [25, 26]. It is convenient to drop charge, mass and amplitude of the oscillator and normalize all self-energy components by Γ_0^r for evaluations, where $\Gamma_0^r = \frac{2\sqrt{\epsilon_o}\mu^2 k^3}{3\hbar}$ and μ is the electric dipole moment of the emitter; k , ϵ_o and \hbar are the wave number, free-space permittivity and reduced Planck's constant.

This widely used conventional description of the self-interaction in equation (3) includes an implicit rotating wave approximation ($|\Re(\Sigma)| \ll \omega$). In the supplementary [27], we confirm that this conventional approximation does not alter the conclusions for the cases discussed in this paper. The non-classical path B and its interference can also make dynamics of the emission non-Markovian i.e. exponentially damped oscillatory decay for a single excitation, which manifests as a multi-exponential decay in ensembles [28, 29]. Since the coupling strengths are moderate in our examples here, we need not normalize the total decay rates for these marginal effects. The real part of self-energy in equation (3) represents the coupling strength 'g' and also energy split ΔE between the two modes of the strongly coupled oscillators [30, 31]:

$$\Omega = 2g = 2|\Re(\Sigma)| = \frac{\Delta E}{\hbar} \quad (4)$$

Note that Rabi frequency Ω used here should be distinguished from the generalized Rabi frequency Ω_o which includes the effects of dephasing, both due to asymmetry in damping of the two oscillators and detuning of resonance frequencies of the two strongly coupled oscillators [32–36].

$$\Omega_o = \frac{1}{4} \sqrt{\Omega^2 - (\Gamma - \Gamma_o)^2 + 4\delta^2} \quad (5)$$

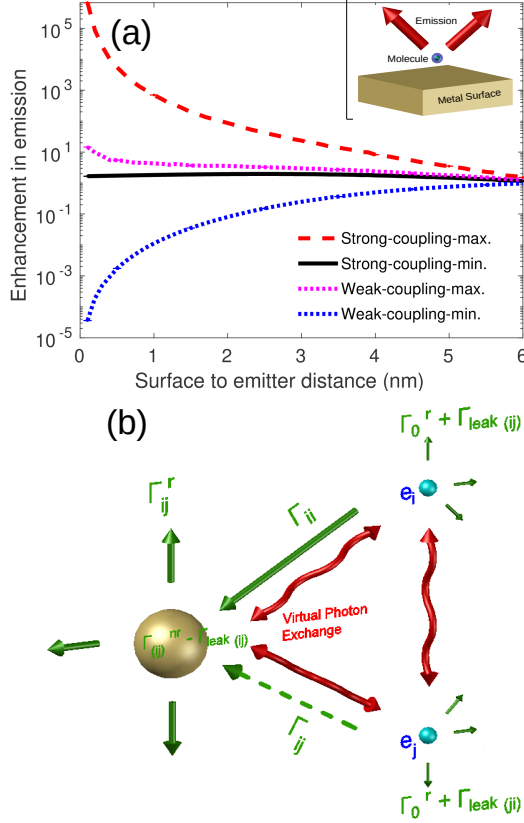


FIG. 2. (a) Enhancements in the proposed theory and the weak-coupling approximation for an emitter near a resonant plane metal surface (relative permittivity $\epsilon \approx -1$). Minimum (Q/Q_o) is given by increase in quantum efficiency defined in equation (14) and the maximum ($Q\Gamma/Q_o\Gamma_o$) represents increase in photon counts due to continuous excitation. (b) The strong-coupling model extended to multiple emitters.

Where the detuning of the emitter from the plasmon resonance of the object is $\delta = \omega_o - \omega_{pl}$.

In figure 2a we show the effect of the above modified partition of optical states, given by equation 2, for spontaneous emission very near a strongly absorbing surface [11]. For larger separations on the order of a wavelength that are not captured in this figure, the strong and weak coupling predictions of quantum efficiency are indistinguishable and display an oscillatory behavior. But very proximal to the surface, only the predictions with the non-classical paths B through the metal yield emission gains large enough to multiply with the enhancement in near-field excitation intensity ($\sim 10^5$) and produce the observed large gains greater than 10^{10} in SERS.

The significant question of interest here is if this coherence of non-classical paths survive when multiple dipole emitters are strongly coupled to metal nanoparticles. This is practically significant as bulk materials have many emitters and even single emitters like quantum dots have a finite size effect on the coupling [12]. We are especially interested in the extremely small metal nanoparti-

cles which have a negligible scattering efficiency and are fully absorbing; see the appendix for the variation of the strength of coupling with size of metal nanoparticles. In the rest of this paper we use a model of many strongly coupled dipole emitters and metal particles, both with and without the non-classical paths described above, to elucidate the density of optical states in such materials.

A coupled system of Lorentz dipole oscillators was used to model an excitation of one quantum of energy shared among N emitters, along with coupled metal nanoparticles (figure 2b). It represents weak excitations given by superpositions of any one excited emitter among the N emitters i.e. the $W_{1,N-1}$ states [37, 38], as required for the study here. This model was first treated analytically under long-wavelength approximations for a spherical metal particle [30], was extended to retarded waves [39], and also to arbitrary geometries without long-wavelength approximations [40]. The pair-wise self-energy contribution of N coupled Lorentz dipole oscillators proximal to metal nanostructure is:

$$\Sigma_{jk}^{total}(\omega) = \frac{-2\pi q^2 \omega}{mc^2} \mathbf{e}_j \cdot \mathbf{G}(\mathbf{r}_j, \mathbf{r}_k; \omega) \cdot \mathbf{e}_k - \delta_{jk} \frac{i\Gamma_o}{2} \quad (6)$$

$$= \Delta_{jk}^{total} - \frac{i\Gamma_{jk}^{total}}{2} \quad (7)$$

Δ_{jk}^{total} and Γ_{jk}^{total} represent entries of $N \times N$ matrices. Each component of matrix $\Delta_{jk} = \Re(\Sigma_{jk}^{total})$ represents the virtual photon exchange between two dipoles at position \mathbf{r}_j and \mathbf{r}_k in presence of metal nanostructure and matrix $\Gamma_{jk} = -2\Im(\Sigma_{jk})$ represents effects of the coupling on decay rates of the two dipole emitters. Green dyadic \mathbf{G} represents interaction between the two dipole emitters in the presence of the metal nanostructure.

The self-energy matrix evaluated in equation (6) is also further decomposed into its metallic contribution Σ and the contribution due to direct interaction among the N coupled dipoles in the absence of metal nanostructures Σ^o .

$$\Sigma_{jk}^{total}(\omega) = \Sigma_{jk}^o(\omega) + \Sigma_{jk}(\omega) \quad (8)$$

where \mathbf{G}_m replaces \mathbf{G} in equation (6) and the second term with Γ_o is ignored, to evaluate $\Sigma_{jk}(\omega)$. \mathbf{G}_m , the metallic contribution of green dyadic is calculated by subtracting \mathbf{G}_o representing free-space interaction between the dipoles in the absence of metal nanostructures, from the total green dyadic \mathbf{G} . \mathbf{G}_o is calculated using the solutions of point source in a homogeneous background:

$$\nabla \times \nabla \times \mathbf{G}_o(\mathbf{r}, \mathbf{r}_j; \omega) - k^2 \mathbf{G}_o(\mathbf{r}, \mathbf{r}_j; \omega) = \mathbf{I} \delta(\mathbf{r} - \mathbf{r}_j). \quad (9)$$

where \mathbf{I} is a unit dyad, the wave number $k = \sqrt{\epsilon} \frac{\omega}{c}$, and $\delta(\mathbf{r} - \mathbf{r}_j)$ represents the point source. This gives us the dyadics for direct interaction among the point-dipoles:

$$\mathbf{G}_o(\mathbf{r}_i, \mathbf{r}_j; \omega) = (\mathbf{I} + \frac{\nabla \nabla}{k^2}) g(|\mathbf{r}_i - \mathbf{r}_j|) \quad (10)$$

where $g(r) = \frac{e^{ikr}}{4\pi r}$. The details of calculation of \mathbf{G} for an arbitrary structure using such dipole granules was shown

elsewhere [40]. The total decay rate Γ in the metal is decomposed into its radiative (Γ^r) and non-radiative (Γ^{nr}) by a factorization of the dyads \mathbf{G} using real and imaginary parts of polarizability of dipole granules, which represent the metal nanoparticle in this volume integral approach.

The eigenstates of the coupled many emitter-metal system are calculated using:

$$\Sigma^{total}|J\rangle = \Delta_J - i\frac{\Gamma_J}{2}|J\rangle \quad (11)$$

Specifically, eigenvectors J represent one of N modes of emission here. The imaginary part of an eigenvalue of Σ^{total} represents decay rate of the mode while the real part of the eigenvalue represents the energy shift. The energy shifts ΔE_J of a collective mode can also be evaluated.

$$\hbar\Omega_J = 2\Delta E_J = 2\hbar|\Delta_J| \quad (12)$$

Note that $|J\rangle$ is not an eigenstate of Σ that represents only the metallic contribution. We evaluate contributions of the metal to the energy shifts and decay rates of a mode using an entry-wise decomposition of Σ_{jk} for all ‘ j ’ and ‘ k ’, into $\Delta_{jk} - i\Gamma_{jk}/2$ and corresponding expectations $\langle J|\Delta|J\rangle$ and $\langle J|\Gamma|J\rangle$. The strength of coupling between emitters through the metal is given by $K_{jk} = 2|\Delta_{jk}|/\Gamma_{jk}$ and its expectation $\langle J|K|J\rangle$ averaged over $|J\rangle$ represents the significance of non-classical metallic paths for the system (figure 3b). Similarly, the strong-coupling correction to the partition of the decay rate is given by entries of a matrix Γ_{jk}^{leak} calculated as:

$$\Gamma_{jk}^{leak} = e^{-\frac{\Gamma_{jk}}{2\Delta_{jk}}} \cdot \Gamma_{jk}^{nr(1)} \quad (13)$$

Here the superscript (1) refers to the dipole mode contribution of the metal nanoparticles. The mode-wise Γ_{leak} is calculated by the expectation $\langle J|\Gamma_{leak}|J\rangle$. The effective decay rates of a mode remain as given in equation (2). The quantum efficiency of a mode and the expected quantum efficiency are given by:

$$Q_J = \frac{\Gamma_{eff}^r}{\Gamma_{eff}^r + \Gamma_{eff}^{nr}} \quad Q = \frac{1}{N} \sum_{J=1}^N Q_J \quad (14)$$

For our analysis of results, let ρ be a measure of coupling of emitters with metal nanoparticles, and it is defined as:

$$\rho = \frac{n_{nc} + n_c}{l_{nc} + l_c + n_{nc} + n_c} \quad (15)$$

where n represents the number of paths through the metal and l represents paths only through the emitters; subscripts c and nc indicate classical and non-classical paths respectively. ρ_{nc} is a measure of strong coupling of the emitters with metal nanoparticles through Rabi oscillations while ρ_c is a measure of its weak coupling, and

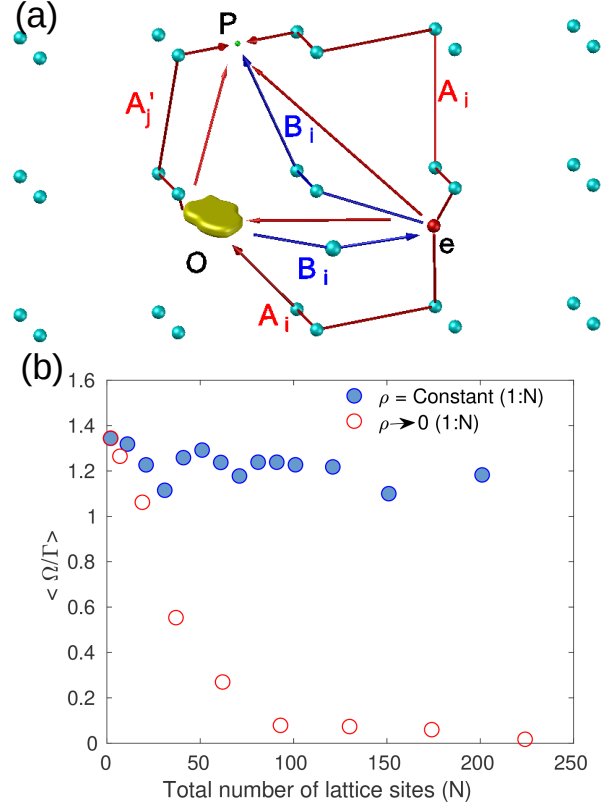


FIG. 3. (a) Strong-coupling of emitters and a metal particle: non-classical paths A_i through other emitters as well as paths B_i through Rabi oscillation with the metal particle are included. (b) Coupling strength of emitters with metal given by the expected ratio of Rabi frequency and decay rate.

they include only n_{nc} or n_c respectively in the numerator of equation (15). In the weak coupling regime $\rho_{nc} = 0$, while in strong coupling regime both ρ_c and ρ_{nc} are non-zero. We investigate two conditions in each of the two cases. Case I: $\rho_{nc} = 0$; (a) $\rho = \text{constant}$ and (b) $\rho \rightarrow 0$. Case II: $\rho_{nc} \neq 0$; (a) $\rho = \text{constant}$ and (b) $\rho \rightarrow 0$. In both cases distinguished in figure 3a, condition (a) represents an increase in the number of emitters within a constant area, while condition (b) represents a case of increase in the number of emitters with a constant area density. See appendix for a description of the geometries used in these cases.

In case I, the emitters are strongly coupled among themselves [41] but the weak coupling approximation with the metal particle is used. This leads to a predicted quenching of emission and a reduction in quantum efficiency as shown in figure 4a. The predicted quenching is similar to the case of single emitter weakly coupled to the metal nanoparticle, and the evaluated coupling strengths shown in figure 3b indicate the breakdown of this approximation. This quenching is constant when the number of emitters increase in a constant area as $\rho = \rho_c$ is constant. When the system expands with a constant area density of emitters, this quenching decreases as does the frac-

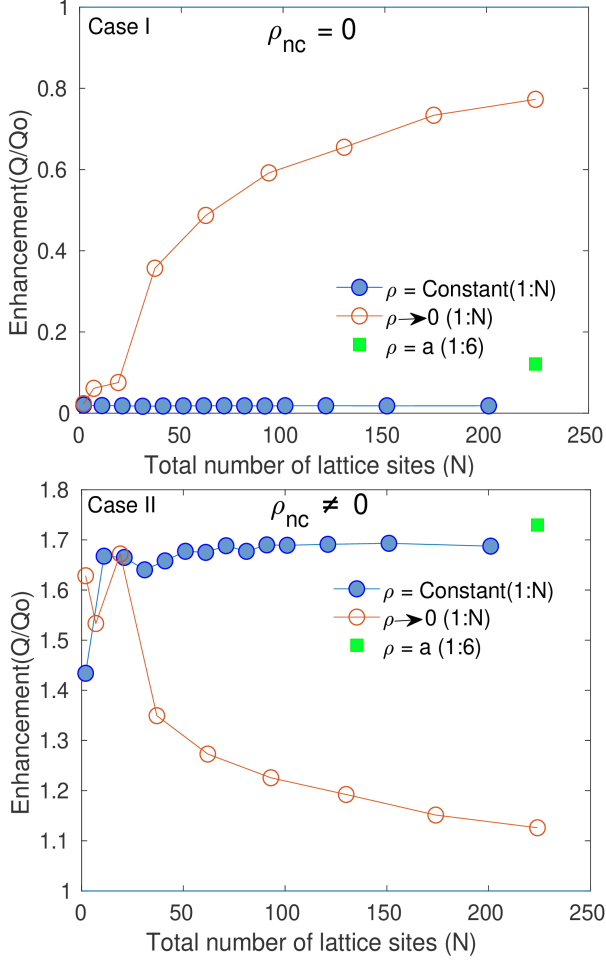


FIG. 4. Modified emission due to gold nanoparticles 1.9 nm in radii at $\lambda = 560$ nm in free-space and $Q_o=0.33$; additional information provided in [27] (I) quenching when only classical paths of the metal are included (II) enhancements when non-classical paths of metal are also included.

tion of paths through the metal particle. When some of the emitters are replaced by metal particles in the model (to reach a ratio of 1:6 for number of metal particles and emitters), quenching of the weak coupling approximation is regained even when this system has now an extended area with many coupled emitters and metal particles.

In case II, emitters are strongly coupled among themselves as well as with a metal particle. There exists non-classical paths among emitters as well as between emitters and the metal nanoparticle, and this leads to enhancements in the quantum efficiency (figure 4b). This enhancement is constant as the number of emitters increase in a constant area, as both ρ_c and ρ_{nc} remain roughly constant. When the system is expanded with a constant area density of emitters $\rho_{nc} \rightarrow 0$ due to weaker couplings, as does ρ_c . The former results in a loss of coherence of non-classical paths B through the metal particle, and the lost enhancement is only regained when some of the emitters are replaced by metal nanoparticles

fixing a ratio of 1:6 for the metal nanoparticles and the emitters.

From the above two cases studied, we can infer that the coherence of non-classical paths among many strongly coupled emitters and metal nanoparticles is sustained independent of the number of emitters and metal particles. This effect diminishes only when a large fraction of emitters are weakly coupled to the metal nanoparticle i.e. when separations between the emitters and a lone metal particle increase. Considering the low dissipative loss of these very small metal particles they are expected to be much more effective in enhancement of spontaneous emission, compared to the larger metal particles required in the weak coupling regime. Further, the emerging coherence in the dynamics of emission in such materials can be gainfully exploited for applications other than light generation [42].

ACKNOWLEDGMENTS

K.J. and M.V. thank the department of Computational & Data Sciences, Indian Institute of Science for its generous support.

Appendix A: Details of simulations

Here we explain additional details of geometries corresponding to $\rho = \text{Constant}$ and $\rho \rightarrow 0$ used for simulations in figure 3 and 4 of the main paper. The emission wavelength of emitters is 560 nm in free-space and the refractive index of surrounding medium is 1.5. $Q_o=0.33$ was assumed without loss of generality. We used gold nanoparticles of diameter 3.8 nm coupled to many dipole emitters.

1. Constant area : $\rho = \text{constant}$

Here we consider $N-1$ dipole emitters around a multipole metal nanoparticle of diameter 3.8 nm (consisting of 552 dipoles) at an average distance of $h=3.5$ nm from the surface of the nanoparticle as shown in figure S1. The point dipole emitters are uniformly distributed in a fixed area of shell of 2 nm. We compute the decay rates with increasing number of emitters in the shell to observe the effect of non-classical interactions with metal nanoparticle, both in weak and strong coupling regime. The quantum efficiency is roughly constant with the increase of number of emitters as shown in figures 4a (quenching by weak coupling) and 4b (enhancement by strong coupling) of the main paper. Note that both non-classical paths only through other emitters l_{nc} , and coherent classical paths through metal n_c increase as a factorial of N . But so does the non-classical paths through metal nanoparticle n_{nc} due to Rabi oscillations among the metal and

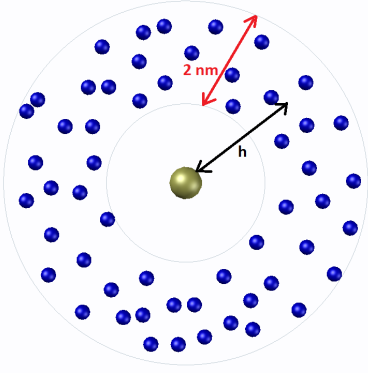


FIG. A1. This geometry represents emitters distributed in constant area (A1). The golden sphere is a gold nanoparticle of radius 1.9 nm. Blue spheres represents dipole emitters where h is average distance between emitters and the nanoparticle.

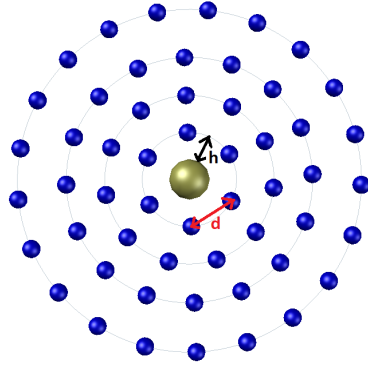


FIG. A2. This geometry represents emitters distributed in constant area density (A2). The golden sphere is a gold nanoparticle of radius 1.9 nm. Blue spheres represents dipole emitters where h is distance between nearest emitters and the nanoparticle.

emitters, in case II. The latter is possible as the strong-coupling of all emitters with the metal is ensured in this geometry. While the classical direct paths l_c increase only linearly with N . This ensures that the fraction of metallic paths $\rho \approx \text{constant}$.

2. Constant area density : $\rho \rightarrow 0$

Here we consider $N-1$ dipole emitters around a multipole metal nanoparticle (consisting of 552 dipole grains) of diameter 3.8 nm, where distances among emitters are fixed so that number of emitters per unit area i.e. area density is constant (see figure S2). The first emitter is

placed at a distance of $h=3.5$ nm from the surface of the metal nanoparticle and then more emitters are added on lattice sites which are at $d \approx 5.5$ nm apart from each other. The lattice sites are located in concentric circles around metal nanoparticle and distance between them is chosen so that first circle around metal contains exactly 6 emitters which may represent a hexagonal lattice. Note that the non-classical paths only through other emitters l_{nc} increase as a factorial of N , while in case II the coherent non-classical paths n_{nc} through Rabi oscillation with metal marginally increases with N to a constant, beyond which emitters are not coupled strongly enough to the metal. The classical paths n_c due to a weak coupling increase as a factorial of N initially, but as the couplings reduce further it converges to a constant when the farther emitters are not coherently coupled to the metal. While the classical direct paths of an emitter to metal l_c increases only linearly with N . This results in the fraction of metallic paths $\rho \rightarrow 0$ as N increases.

The quantum efficiency increases towards the free-space value ($Q/Q_o = 1$) with number of emitters added as shown in figure 4a (for weak coupling) and the enhancement decreases in 4b (strong coupling) towards the free-space value. We also show that this quantum efficiency again increases when some of the random emitters are replaced by metal nanoparticles on same lattice sites so that overall metal to lattice sites ratio is 1:6. So green squares in figures 4 of the main paper show the qualitative behaviour of this model (B) on adding more metal nanoparticles to replace the emitters. The green squares show simulations for 224 lattice sites out of which 32 are metal nanoparticles. Note that we used dipole metal nanoparticles to model this special case because of computational complexity of the multipole nanoparticle. Each data point in the figures involve a number of simulations of many random configuration of polarizations and permuted positions, numbering greater than N until the relative variation in the expected value is small.

Appendix B: Coupling strengths and size of gold nanoparticles

A larger factor $e^{-\Gamma/\Omega}$, determines the degree of divergence of observations from the predictions of weak matter-coupling approximation. Variation of this exponent in a logarithmic scale are plotted below for a fixed small distance of 3 nm and for a ‘relative’ distance fixed as the radius ‘R’ of metal particle. These figures B1 and B2 provide insight into the strong-coupling effects and the size of metal particles. All the above cases represent gold nanoparticles with a surrounding medium of refractive index 1.5, and at a free-space wavelength of 560 nm.

[1] Y. Zhu, D. J. Gauthier, S. E. Morin, Q. Wu, H. J. Carmichael, and T. W. Mossberg, Phys. Rev. Lett. **64**,

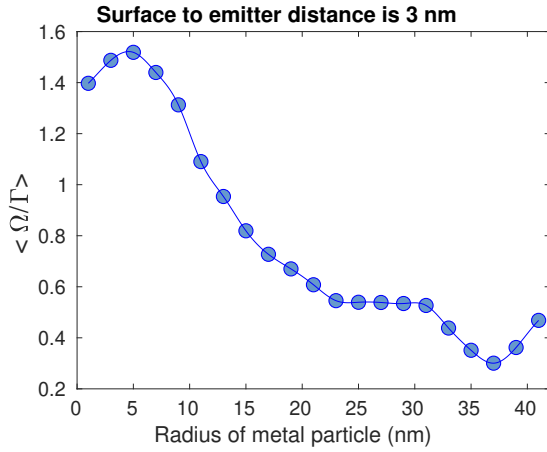


FIG. B1.

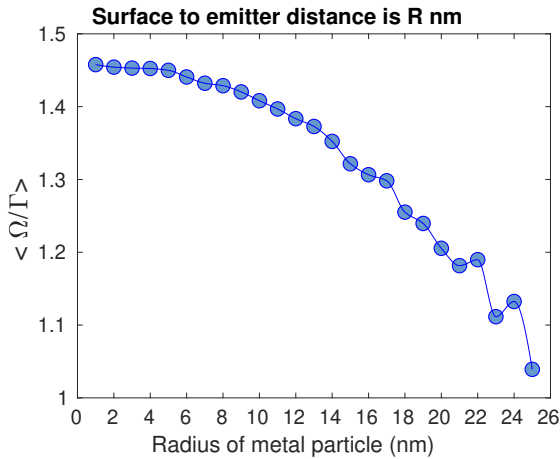


FIG. B2.

- [2] F. Bernardot, P. Nussenzveig, M. Brune, J. M. Raimond, and S. Haroche, *Europhys. Lett.* **17**, 33 (1992).
- [3] A. Boca, R. Miller, K. M. Birnbaum, A. D. Boozer, J. McKeever, and H. J. Kimble, *Phys. Rev. Lett.* **93**, 233603 (2004).
- [4] T. Yoshie, A. Scherer, J. Hendrickson, G. Khitrova, H. M. Gibbs, G. Rupper, C. Ell, O. B. Shchekin, and D. G. Deppe, *Nature* **432**, 200 (2004).
- [5] J. Bellessa, C. Bonnand, J. C. Plenet, and J. Mugnier, *Phys. Rev. Lett.* **93**, 036404 (2004).
- [6] G. Zengin, M. Wersäll, T. J. Nilsson, S. Antosiewicz, M. Kall, and T. Shegai, *Phys. Rev. Lett.* **114**, 157401 (2015).
- [7] A. E. Schlather, N. Large, A. S. Urban, P. Nordlander, and N. J. Halas, *Nano Lett.* **13**, 3281 (2013).
- [8] N. Vats, S. John, and K. Busch, *Phys. Rev. A* **65**, 043808 (2002).
- [9] D. E. Chang, A. S. Sørensen, P. R. Hemmer, and M. D. Lukin, *Phys. Rev. B* **76**, 035420 (2007).
- [10] A. Delga, J. Feist, J. Bravo-Abad, and F. J. Garcia-Vidal, *Phys. Rev. Lett.* **112**, 253601 (2014).
- [11] K. Jain and M. Venkatapathi, *Phys. Rev. Appl.* **11**, 054002 (2019).
- [12] R. Dutta, K. Jain, M. Venkatapathi, and J. K. Basu, *Phys. Rev. B* **100**, 155413 (2019).
- [13] G. C. Schatz, M. A. Young, and R. P. Van Duyne, in *Surface-enhanced Raman scattering* (Springer, 2006) pp. 19–45.
- [14] M. Moskovits, *Phys. Chem. Chem. Phys.* **15**, 5301 (2013).
- [15] K. Kneipp, *J. Phys. Chem. C* **120**, 21076 (2016).
- [16] M. Haridas and J. K. Basu, *Nanotechnol.* **21**, 415202 (2010).
- [17] M. Haridas, J. K. Basu, D. J. Gosztola, and G. P. Wiederrecht, *Appl. Phys. Lett.* **97**, 189 (2010).
- [18] K. A. Kang, J. Wang, J. B. Jasinski, and S. Achilefu, *J. Nanobiotechnol.* **9**, 16 (2011).
- [19] M. Haridas, J. K. Basu, A. K. Tiwari, and M. Venkatapathi, *J. Appl. Phys.* **114**, 064305 (2013).
- [20] M. Macovei, J. Evers, G.-x. Li, and C. H. Keitel, *Phys. Rev. Lett.* **98**, 043602 (2007).
- [21] V. Shatokhin, C. Müller, and A. Buchleitner, *Phys. Rev. Lett.* **94**, 043603 (2005).
- [22] A. Safari, R. Fickler, E. Giese, O. S. Magaña-Loaiza, R. W. Boyd, and I. De Leon, *Phys. Rev. Lett.* **122**, 133601 (2019).
- [23] L. Novotny, *Am. J. Phys.* **78**, 1199 (2010).
- [24] M. Venkatapathi, *J. Quant. Spectros. Radiat. Transfer* **113**, 1705 (2012).
- [25] J. Tignon, P. Voisin, C. Delalande, M. Voos, R. Houdré, U. Oesterle, and R. P. Stanley, *Phys. Rev. Lett.* **74**, 3967 (1995).
- [26] V. Debierre, T. Durt, A. Nicolet, and F. Zolla, *Phys. Lett. A* **379**, 2577 (2015).
- [27] Supplementary material at [URL will be inserted by publisher] for additional information on simulated results (2020).
- [28] K. H. Madsen, S. Ates, T. Lund-Hansen, A. Löffler, S. Reitzenstein, A. Forchel, and P. Lodahl, *Phys. Rev. Lett.* **106**, 233601 (2011).
- [29] A. Gonzalez-Tudela, F. J. Rodríguez, L. Quiroga, and C. Tejedor, *Phys. Rev. B* **82**, 115334 (2010).
- [30] V. N. Pustovit and T. V. Shahbazyan, *Phys. Rev. B* **82**, 075429 (2010).
- [31] A. Schülzgen, R. Binder, M. Donovan, M. Lindberg, K. Wundke, H. Gibbs, G. Khitrova, and N. Peyghambarian, *Phys. Rev. Lett.* **82**, 2346 (1999).
- [32] G. S. Agarwal, *J. Opt. Soc. Am. B* **2**, 480 (1985).
- [33] H. Kamada, H. Gotoh, J. Temmyo, T. Takagahara, and H. Ando, *Phys. Rev. Lett.* **87**, 246401 (2001).
- [34] M. Pelton, S. D. Storm, and H. Leng, *Nanoscale* **11**, 14540 (2019).
- [35] F. Alpeggiani, S. D'Agostino, and L. C. Andreani, *Phys. Rev. B* **86**, 035421 (2012).
- [36] F. Alpeggiani, S. D'Agostino, and L. C. Andreani, in *2014 16th International Conference on Transparent Optical Networks (ICTON)* (IEEE, 2014) pp. 1–4.
- [37] A. A. Svidzinsky, J. Chang, and M. O. Scully, *Phys. Rev. A* **81**, 053821 (2010).
- [38] R. Wiegner, J. Von Zanthier, and G. S. Agarwal, *Phys. Rev. A* **84**, 023805 (2011).
- [39] C. Van Vlack, P. T. Kristensen, and S. Hughes, *Phys. Rev. B* **85**, 075303 (2012).
- [40] M. Venkatapathi, *J. Opt. Soc. Am. B* **31**, 3153 (2014).
- [41] L. Jin, J. Evers, and M. Macovei, *Phys. Rev. A* **84**, 043812 (2011).
- [42] M. Otten, R. A. Shah, N. F. Scherer, M. Min, M. Pelton, and S. K. Gray, *Phys. Rev. B* **92**, 125432 (2015).